Spectrochimica Acta Part A 82 (2011) 444–455

Contents lists available at ScienceDirect

Spectrochimica Acta Part A: Molecular and Biomolecular Spectroscopy

journal homepage: www.elsevier.com/locate/saa

Synthesis, molecular conformation, vibrational and electronic transition, isometric chemical shift, polarizability and hyperpolarizability analysis of 3-(4-Methoxy-phenyl)-2-(4-nitro-phenyl)-acrylonitrile: A combined experimental and theoretical analysis

Abdullah Mohamed Asiri[a,b], Mehmet Karabacak[c,*], Mustafa Kurt[d], Khalid A. Alamry[a]

[a] Department of Chemistry, Faculty of Science, King Abdul Aziz University, Jeddah 21413, 80203, Saudi Arabia
[b] The Center of Excellence for Advanced Materials Research, King Abdul Aziz University, Jeddah 21589, 80203, Saudi Arabia
[c] Department of Physics, Afyon Kocatepe University, 03040, Afyonkarahisar, Turkey
[d] Department of Physics, Ahi Evran University, 40100, Kırşehir, Turkey

ARTICLE INFO

Article history:
Received 16 March 2011
Received in revised form 18 July 2011
Accepted 21 July 2011

Keywords:
FT-IR
UV–vis
^{13}C and ^{1}H NMR
NLO
DFT

ABSTRACT

This work presents the synthesis and characterization of a novel compound, 3-(4-Methoxy-phenyl)-2-(4-nitro-phenyl)-acrylonitrile (abbreviated as 3-(4MP)-2-(4-NP)-AN, $C_{16}H_{12}N_2O_3$). The spectroscopic properties of the compound were examined by FT-IR, UV–vis and NMR (^{1}H and ^{13}C) techniques. FT-IR spectrum in solid state was observed in the region 4000–400 cm^{-1}. The UV–vis absorption spectrum of the compound which dissolved in chloroform was recorded in the range of 200–800 nm. The ^{1}H and ^{13}C NMR spectra were recorded in $CDCl_3$ solution. To determine lowest-energy molecular conformation of the title molecule, the selected torsion angle is varied every 10° and molecular energy profile is calculated from 0° to 360°. The structural and spectroscopic data of the molecule in the ground state were calculated using density functional theory (DFT) employing B3LYP/6-31G(d,p) basis set. The dipole moment, linear polarizability and first hyperpolarizability values were also computed using the same basis set. A study on the electronic properties, such as HOMO and LUMO energies, were performed by time-dependent DFT (TD-DFT) approach. The HOMO and LUMO analysis were used to elucidate information regarding charge transfer within the molecule. The vibrational wavenumbers were calculated and scaled values were compared with experimental FT-IR spectrum. The complete assignments were performed on the basis of the experimental results and total energy distribution (TED) of the vibrational modes, calculated with scaled quantum mechanics (SQM) method. Isotropic chemical shifts were calculated using the gauge-invariant atomic orbital (GIAO) method. Comparison of the calculated frequencies, NMR chemical shifts, absorption wavelengths with the experimental values revealed that DFT and TD-DFT method produce good results. The linear polarizabilities and first hyperpolarizabilities of the studied molecule indicate that the title compound can be used as a good nonlinear optical material. The thermodynamic properties of the studied compound at different temperatures were calculated, revealing the correlations between standard heat capacity, standard entropy, standard enthalpy changes and temperatures.

1. Introduction

Organic photochromic compounds having donor and acceptor parts that are conjugated are potential optical materials. Donor–acceptor (D–π–A) dyestuff and colorants represent a vast majority of organic chromogens. Such compounds have found many applications such as in dyeing of fabric, coloring of toners, and in image forming and optical information storage technologies. Some of these compounds are also used as sources of tunable (dye laser) radiation [1–3].

Theoretical investigations can facilitate the solution to the problems confronted in the experimental techniques, i.e. allowing the determination of molecular properties. The calculations based on DFT have been applied in many areas, and the results also are in great agreement with the experimental ones in calculating spectroscopic properties [4–6]. The calculated harmonic frequencies are usually higher than the corresponding experimental quantities, due to a combination of electron correlation effects and basis set deficiencies. DFT calculations are reported to provide excellent vibrational frequencies of organic compounds if the calculated

* Corresponding author. Tel.: +90 272 2281311; fax: +90 272 2281235.
E-mail address: karabacak@aku.edu.tr (M. Karabacak).

1386-1425/$ – see front matter © 2011 Elsevier B.V. All rights reserved.
doi:10.1016/j.saa.2011.07.076

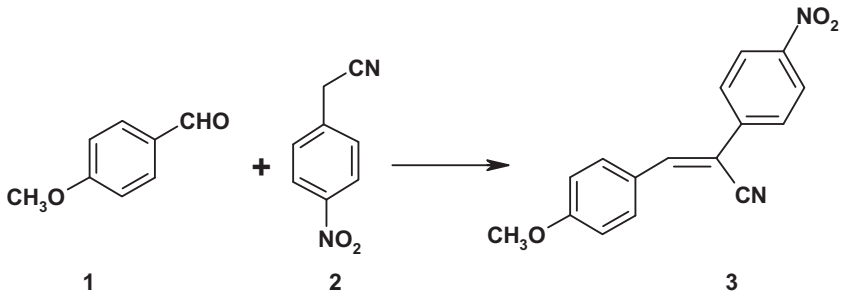

Scheme 1. Synthesis of 3-(4MP)-2-(4-NP)-AN.

frequencies are scaled to compensate for the approximate treatment of electron correlation [7–9].

We synthesized benzylidene based on cyclopentanone and its cyclpentylidene malononitrile condensate [10]. The purpose of the present study is to show the results of FT-IR, UV–vis and NMR spectra and to calculate optimal molecular geometry, vibrational frequencies and normal modes associated of 3-(4MP)-2-(4-NP)-AN compound (Scheme 1). The geometric structure, HOMO–LUMO energies, absorption wavelengths, excitation energies, vibrational frequencies, ^{1}H and ^{13}C NMR chemical shifts of title molecule were studied by using Gaussian 03 suite of quantum chemical codes [11], for the first time. The HOMO and LUMO analysis have been used to elucidate information regarding charge transfer within the molecule. A detailed quantum chemical study was aid in making definite assignments to fundamental normal modes of 3-(4MP)-2-(4-NP)-AN and in clarifying the experimental data for this important molecule. A detailed interpretation of the vibrational spectra of title molecule has been made on the basis of the calculated total energy distribution (TED). These experimental and calculated values are valuable for providing insight into the vibrational, UV–vis, NMR spectrum and molecular parameters. Besides these, the dipole moments, nonlinear optical properties (NLO), linear polarizability and first hyperpolarizability, and thermodynamic properties were also studied. The results obtained from theoretical calculations and experiments were compared.

2. Materials and methods

2.1. Materials and synthesis of 3-(4-Methoxy-phenyl)-2-(4-nitro-phenyl)-acrylonitrile

4-Methoxybenzaldehyde (1.5 g, 0.011 mol) and 4-nitrophenylacetonitrile (1.78 g, 0.011 mol) were dissolved in 30 ml of ethanol then heated to boiling before Pipyridine (0.5 ml) was added. The reaction mixture was refluxed for 4 h, cooled then the precipitate was filtered and recrystallized from ethanol.

Yield: 90%
Melting Point: 194–196 °C
Colour: Yellow
FT-IR (KBr disk) *wavenumbers* (ν; cm^{-1}): 3086, 2941, 2842 (–C–H), 2213 (CN), 1580, 1512 (C=C), 1512, 1332 (NO_2), 1263 (C–O).
UV–vis ($CHCl_3$): λ_{max}/nm (log ε) 378 (5.17).
^{1}H NMR; ($CDCl_3$ d6) δ 8.33(dd, 2H, J = 8.8 Hz, H aromatic), 7.98 (dd, 2H, J = 9.2 Hz, H aromatic), 7.85 (dd, 2H, J = 9.2 Hz, H aromatic), 7.63 (s, ^{1}H, H olefinic), 7.04 (dd, 2H, J = 8.8 Hz, H aromatic), 3.92 (s, 3H, OCH_3).
^{13}C NMR; ($CDCl_3$ d6) 162.37, 147.45, 145.06, 141.08, 131.96, 126.33, 125.65, 124.34, 117.77, 114.64, 106.1, 55.56.
Elemental analysis: Calculated for $C_{16}H_{12}N_2O_3$: C; 68.57%, H; 4.32%, N; 9.99%; Found: C; 68.43%, H; 4.28%, N; 9.83%.

2.2. Experimental details

The FT-IR spectrum of molecule was recorded in the region 400–4000 cm^{-1} on a Perkin Elmer FT-IR System Spectrum BX spectrometer calibrated using polystyrene bands. The sample was prepared using a KBr disc technique because of solid state. The UV–vis absorption spectrum of title molecule was examined in the range 200–800 nm using Shimadzu UV-2401 PC, UV–vis recording Spectrometer. The UV pattern is taken from a 10^{-5} molar solution of 3-(4MP)-2-(4-NP)-AN, dissolved in chloroform. NMR experiments were performed in Brucker DPX 600 MHz at 300 K. The compound was dissolved in $CDCl_3$. Chemical shifts were reported in ppm relative to tetramethylsilane (TMS) for ^{1}H and ^{13}C NMR spectra. ^{1}H and ^{13}C NMR spectra were obtained at a base frequency of 600 MHz and 150 MHz, respectively.

2.3. Quantum chemical calculation

The first task for the computational work was to determine the optimized geometry of the compound. To determine conformational features of the molecule, the selected degree of torsional freedom, T (C2–C1–C16–C18), was varied from 0° to 360° in every 10° and the molecular energy profile was obtained with the B3LYP/6-31G (d,p) method. Analytic frequency calculations at the optimized geometry were done to confirm the optimized structures to be an energy minimum and to obtain the theoretical vibrational spectra. At the optimized geometry for the title molecule no imaginary frequency modes were obtained, so there is a true minimum on the potential energy surface is found. It is well known in the quantum chemical literature that the hybrid B3LYP [12,13] method based on Becke's three parameter functional of DFT yields a good description of harmonic vibrational wavenumbers for small and medium sized molecules.

Based on our previous experience [4,7,14] this method and a fairly large and flexible basis set 6-31G(d,p) level to perform accurate calculations on the title molecule were chosen. However, the frequency values computed at these levels contain known systematic errors [15]. We know that DFT potentials symmetrically overestimate the vibrational wavenumbers. These discrepancies are corrected either by computing an harmonic corrections explicitly [16] or by introducing a scaled field or by directly scaling the calculated wavenumbers with a proper factor. Considering systematic errors with a scaling factor of 0.9608 [17], we calibrated the vibrational wavenumbers calculated by B3LYP method. After scaling with a scaling factor, the deviation from the experiment is more reliable.

TED calculations, which show the relative contributions of the redundant internal coordinates to each normal vibrational mode of the molecule, and thus enable us numerically to describe the character of each mode were carried out by SQM method [18] using the output files created at the end of the frequency calculations. The TED calculations were performed by using PQS program [19].

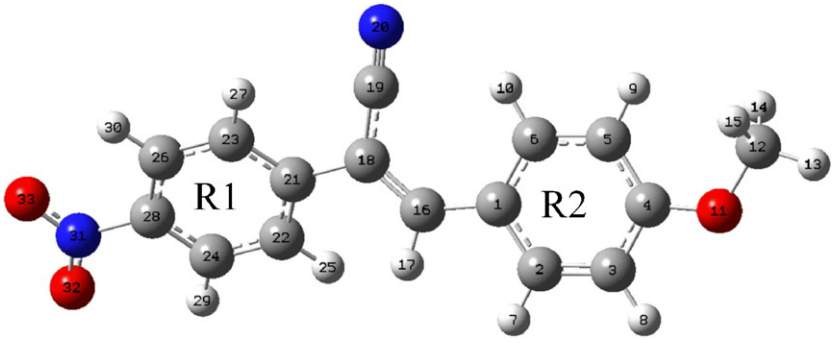

Fig. 1. The theoretical optimized possible geometric structure with atoms numbering of title molecule.

The electronic properties, such as HOMO–LUMO energies, absorption wavelengths and oscillator strengths were calculated using B3LYP method of the time-dependent DFT (TD-DFT), basing on the optimized structure in chloroform and gas phase.

For NMR calculations, the title molecule was firstly optimized with B3LYP method and 6-31G(d,p) level. After optimization, ^{1}H and ^{13}C NMR chemical shifts (δH and δC) were calculated using the GIAO method [20] in gas phase and solution phase (chloroform ($CDCl_3$)). Relative chemical shifts were then estimated by using the corresponding TMS shielding calculated in advance at the same theoretical level as the reference. ^{13}C and ^{1}H isotropic magnetic shielding (IMS) of any X carbon (or hydrogen) atom was made according to the value ^{13}C IMS of TMS: $CS_x = IMS_{TMS} - IMS_x$ (^{1}H IMS of TMS: $HS_x = IMS_{TMS} - IMS_x$). Calculated ^{1}H and ^{13}C isotropic chemical shieldings for TMS at B3LYP methods with 6-31G(d,p) level in $CDCl_3$ by using the IEFPCM method were 31.757 ppm and 192.169 ppm, respectively. The experimental values for ^{1}H and ^{13}C isotropic chemical shifts for TMS were 30.84 ppm and 188.1 ppm, respectively [21].

In order to show NLO activity of the molecule, the dipole moment, linear polarizability and first hyperpolarizability were obtained using the same level of theory. In addition, the changes in the thermodynamic functions the heat capacity, entropy, and enthalpy were investigated for the different temperatures from the vibrational frequencies calculations of title molecule.

3. Results and discussion

The molecule of 3-(4MP)-2-(4-NP)-AN consists of 33 atoms, so it has 93 normal vibrational modes. Its molecular structure has not been studied by any diffraction technique; therefore we have taken into account two different symmetries. We calculated the structural and spectroscopic data of the molecule in the Cs and C_1 point group symmetry. On the assumption of a Cs symmetry the numbers of vibration modes of the 93 fundamental vibrations of title molecule are $63A' + 30A''$. The vibrations of the A' species are in plane and those of the A'' species are out of plane. From DFT calculations with 6-31G(d,p) basis set, because of the imaginary frequency which correspond to R1 (ring 1) wagging perpendicular to the ring plane (A''), the calculations show that Cs point group conformer to be unstable. But if the molecule was C_1 there would not be any relevant distribution and molecule has minimum energy (for example, E(B3LYP) = −951.99382044 a.u. for Cs symmetry and E(B3LYP) = −951.99443126 a.u. for C_1 symmetry). This result shows that, the structure in C_1 symmetry is the lowest in energy. Therefore, the calculated results for C_1 symmetry group were tabulated.

3.1. Molecular geometry and potential energy surface scan

The theoretical structure of the title compound is shown in Fig. 1. The optimized structure parameters (bond lengths and bond angles) of title molecule listed in Table 1 with the X-ray experimental similar molecule [22] for comparison in accordance with the atom numbering scheme given in Fig. 1. The optimized geometrical parameters of the molecule were compared with the X-ray study of the similar molecule reported by Asiri et al. [22].

The equilibrium structure for the ground state shows that one of the methyl C–H bonds is parallel (179.92°) to the ring plane. In nitro group, the nitrogen atom is nearly parallel to the R1 ring plane, with a torsional angle C23–C26–C28–N31 and C22–C24–C28–N31 averaged value 179.88°. Asiri et al. [22] obtained this value 179.23° for similar molecule measure of this displacement is defined the tilt angle [23]. Existence of this angle has been interpreted to be caused by asymmetric interaction between the NO_2 group and benzene ring plane.

The asymmetry of the benzene ring is also evident from the negative deviation of C2–C1–C6, C2–C3–C4 (or C3–C4–C5) which are calculated ca. 117° and 119° positive deviation of the remaining angles from the normal value of 120°. Similar values found to be for other benzene derivatives [4,24,25].

In order to describe conformational flexibility of the title molecule, the energy profile as a function of C2–C1–C16–C18 torsion angle was achieved with B3LYP/6-31G(d,p) method (Fig. 2). According to X-ray crystallographic study torsional angle, T (C2–C1–C16–C18), was determined as 175.78° [22] and in this study the mentioned torsional angle was computed at 175.54° by DFT method. The conformational energy profile shows two maxima near 90° and 270°. The maximum energies are obtained at

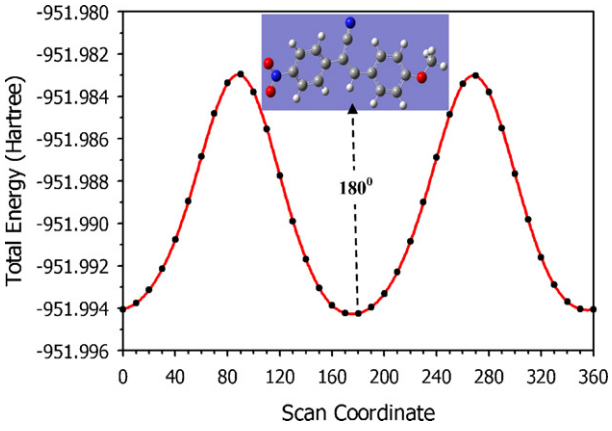

Fig. 2. PES scan for dihedral angle C2–C1–C16–C18 at B3LYP/6-31G(d,p).

Table 1
Optimized geometry using B3LYP/6-31G(d,p) of 3-(4MP)-2-(4-NP)-AN, in the ground state.

	X-ray [22]	DFT	Bond angles (°)	X-ray [22]	DFT
Bond lengths (Å)					
C1–C2	1.400	1.416	C4–C5–C6	120.2	120.1
C1–C6	1.414	1.410	C4–C5–H9	–	120.9
C1–C16	1.450	1.452	C6–C5–H9	–	119.0
C2–C3	1.387	1.382	C1–C6–C5	120.6	121.4
C3–C4	1.388	1.405	C1–C6–H10	119.7	120.4
C4–C5	1.410	1.404	C5–C6–H10	119.7	118.2
C4–O11	1.353	1.355	C4–O11–C12	117.6	118.7
C5–C6	1.381	1.390	C1–C16–H17	114.1	113.0
O11–C12	1.438	1.424	C1–C16–C18	131.8	132.5
C16–H17	0.950	1.087	C18–C16–H17	114.1	114.5
C16–C18	1.355	1.367	C16–C18–C19	121.5	122.1
C18–C19	1.444	1.432	C16–C18–C21	124.1	122.4
C18–C21	1.481	1.485	C19–C18–C21	114.3	115.6
C19–N20	1.148	1.165	C18–C21–C22	121.2	121.4
C21–C22	1.404	1.409	C18–C21–C23	120.8	120.3
C21–C23	1.395	1.408	C22–C21–C23	118.0	118.3
C22–C24	1.381	1.388	C21–C22–C24	121.2	121.1
C23–C26	1.390	1.389	C21–C22–H25	119.4	120.1
C24–C28	1.381	1.394	C24–C22–H25	119.4	118.8
C26–C28	1.381	1.393	C21–C23–C26	121.5	121.1
C28–N31	1.472	1.468	C21–C23–H27	119.3	119.6
N31–O32	1.230	1.232	C26–C23–H27	119.3	119.3
N31–O33	1.226	1.231	C22–C24–C28	118.8	118.9
C–H (R1and R2)[a]	0.950	1.084	C22–C24–H29	120.6	121.6
C–H (Methyl)[a]	0.980	1.094	C28–C24–H29	120.6	119.4
Bond angles (°)			C23–C26–C28	118.2	118.9
C2–C1–C6	118.3	117.2	C23–C26–H30	120.9	121.6
C2–C1–C16	116.8	125.7	C28–C26–H30	120.9	119.5
C1–C2–C3	121.2	121.9	C24–C28–C26	122.2	121.6
C1–C2–H7	119.4	119.1	C24–C28–N31	118.8	119.1
C3–C2–H7	119.4	119.0	C26–C28–N31	119.0	119.3
C2–C3–C4	120.2	119.8	C28–N31–O32	117.8	117.7
C2–C3–H8	119.9	121.5	C28–N31–O33	117.7	117.7
C4–C3–H8	119.9	118.7	O32–N31–O33	124.4	124.6
C3–C4–C5	119.5	119.5	H–C–H (Methyl)[a]	109.5	109.3
C3–C4–O11	115.4	115.8	O–C–H (Methyl)[a]	109.5	109.5
C5–C4–O11	125.0	124.7			

[a] Averaged value.

−951.9829603640 and −951.9830043010 Hartree for 90° and 270° dihedral angles, respectively. The aromatic rings are nearly perpendicular at these values of selected torsion angle. The energy barriers may be due to the steric interactions between the π electrons of the two aromatic rings. It is clear from Fig. 2, there are three local minima observed at 0°, 180° and 360° (−951.9940594110 Hartree for 0°, −951.9942554220 Hartree for 180°, −951.9940594130 Hartree for 360°) for T (C2–C1–C16–C18). Therefore, the most stable conformer is for 180° torsion angle. The DFT optimized geometry of the crystal structure is coplanar at these values of selected torsion angle.

3.2. Vibrational analysis

The experimental FT-IR and the theoretical vibrational spectra (where the calculated intensity is plotted against the vibrational frequencies) of 3-(4MP)-2-(4-NP)-AN are given in Fig. 3 and Fig. S1 (Supplementary Information), respectively. The resulting vibrational frequencies for the optimized geometries and the proposed vibrational assignments as well as IR intensities are given in Table 2. In the last column is given a detailed description of the normal modes based on the total energy distribution (TED). Calculations were made for a free molecule in vacuum, while experiments were performed for solid samples, therefore, there are disagreements between calculated and observed vibrational wavenumbers.

The heteroaromatic structure shows the presence of CH stretching vibrations in the 3000–3100 cm^{-1} range which is the characteristic region for the ready identification of CH stretching vibrations [26]. In this region, the bands are not affected appreciably by the nature of the substituents. Accordingly, in the present study, the eight adjacent hydrogen atoms left around the rings title molecule give rise eight CH stretching modes (86–93), eight CH in plane bending (53, 54, 56, 58, 62, 63, 73, 74) and eight CH out-of-plane bending (37–39, 42, 44–47) vibrations. The vibrations 86–93 assigned to aromatic CH stretching. These modes are calculated from 3059 to 3120 cm^{-1} for title molecule. The other CH stretching mode (C_{16}–H_{17}, mode 85) is computed at 3050 cm^{-1}. In aromatic compounds, CH in plane bending frequencies appear in the range of 1000–1300 cm^{-1} and CH out-of-plane bending vibration in the range 750–1000 cm^{-1} [27]. The CH in plane bends are assigned to the FT-IR bands at 1112 and 1189 cm^{-1} and the out-of-plane bending modes are assigned in the range 961–842 cm^{-1}. Both the in-plane and out-of-plane bending vibrations are described as mixed modes. Additionally, C_{16}–H_{17} atoms have in-plane and out-of-plane bending vibrations (see Table 2).

A major coincidence of theoretical values with that of experimental evaluations is found in the symmetric and asymmetric vibrations of the CH_3 moiety. The asymmetric stretch usually appears at higher wavenumber than the symmetric stretch (vibrations 82 and 83). Therefore, the CH_3 asymmetrical and symmetrical stretching occurs about 2900 and 2800 cm^{-1}, respectively [14,28]. In this study, the symmetric stretching of CH_3 was observed in FT-IR at 2842 cm^{-1} and calculated (mod 82) at 2909 cm^{-1}. The asymmetric CH_3 stretch (mod 83) was calculated and observed at 2974 and 2941 cm^{-1}, respectively. The TED of these modes is 100%. Altun et al. [24] assigned these bands at 2919 and 2857 cm^{-1} for m-methylaniline.

Table 2
Comparison of the calculated and experimental vibrational spectra of 3-(4MP)-2-(4-NP)-AN.

Mode no.	Unscaled Freq.	Scaled Freq.[a]	$I^{Infrared}$	FT-IR	TED[b] (≥10%)
1	24	23	0.3		Γ $CCCC_{R2}$ (60) + Γ $CCCC_{R1}$ (14)
2	28	27	0.5		Γ CC–CC_{R1} (46) + Γ CC–CC_{R2} (30)
3	43	42	1.1		Γ CCCC (43) + β CCC (20)
4	50	48	2.5		ΓNO_2 (25) + Γ CCCC (20) + β CCC (16)
5	71	68	1.3		ΓNO_2 (66) + Γ CCCC (22)
6	80	77	4.2		r CH_3 (26) + β CCC (15)
7	110	106	2.5		r CH_3 (48) + β CCC (13)
8	135	129	4.2		β CCC (38) + Γ CCOC (18) + Γ CCOC (11)
9	151	145	2.3		β $CC_{18}C$ (35) + Γ $CCCN_{20}$ (26)
10	174	167	1.2		Γ $CCCN_{31}$ (15) + r CH_3 (14) + Γ CCCC (11)
11	208	200	1.5		β CCN_{31} (35) + Γ CH_3 (20)
12	232	223	0.2		Γ CH_3 (66)
13	247	237	1.3		Γ CH_3 (40) + β CCN_{31} (19)
14	270	260	0.5		Γ CH_3 (35) + Γ CCCC (10)
15	299	288	3.1		β COC (21) + β CCC (19) + β CCN_{31} (13)
16	339	326	2.8		Γ $CCCN_{20}$ (32) + Γ $CCCC_{R1}$ (14) + Γ CCNO (10)
17	376	361	14.2		ν R_1-NO_2 (30) + β CCC (15)
18	384	369	0.1		Γ $CCCN_{20}$ (18) + β CCC (17)
19	404	388	0.5		Γ $CCCC_{R2}$ (18) + Γ CCCC (18) + β CCC_{18} (15)
20	422	405	0.3		Γ$CCCC_{R1}$ (61) + Γ$CCCH_{R1}$ (23)
21	424	408	0.1		Γ$CCCC_{R2}$ (45) + Γ$CCCH_{R2}$ (20)
22	485	466	1.1		β COC (32) + β CCC_{R2} (10)
23	497	478	5.9		Γ$CCCH_{R1}$ (23) + Γ$CCCC_{R1}$ (14) + ΓCNOO (10)
24	532	511	4.6		r NO_2 (44) + β CCN (10)
25	543	522	13.4		Γ$CCCH_{R2}$ (35) + Γ$CCCC_{R2}$ (18)
26	548	526	0.3		ΓCCCN (22) + β ONC (18) + ν R_1-NO_2 (14) + ν CC_{18} (12)
27	559	537	42.7	531 vs	β (CCO + COC) (28) + β CCC_{R2} (19) + β $CC_{18}C$ (10)
28	643	618	0.8		Ring 1 deformation (56)
29	644	619	1.9		Ring 2 deformation (65)
30	655	629	3.0		Γ CCCC (32) + ΓCCCN (25)
31	708	680	11.5	666 w	Γ $CCCC_{R1}$ (63) + Γ CNOO (15)
32	713	685	4.7	692 w	β CCC_{R1} (13) + ρ NO_2 (10) + β $CC_{18}C$ (10)
33	732	703	3.4		Γ $CCCC_{R2}$ (50) + Γ $CCCH_{R1}$ (22)
34	763	733	14.4	751 s	Γ CNOO (44) + Γ $CCCC_{R1}$ (20)
35	779	749	2.0		β CCC (30) + ν CO (18) + ν CC_{R2} (15)
36	795	764	2.3		β ($C_{19}C_{18}C_{16}$ + $C_{19}C_{18}C_{21}$ + $C_{18}C_{16}C_1$) (35) + ν C_{18}–C_{19} (16)
37	825	793	0.7		γ CH_{R2} (83) + Γ CCCO (10)
38	846	813	37.7		γ CH_{R2} (73)
39	848	815	4.3		γ CH_{R1} (73)
40	858	824	30.1		ν CC_{R2} (24) + β NO_2 (10) + Γ $CCCH_{R1}$ (10)
41	870	836	42.7		ρ NO_2 (39) + ν CC_{R1} (19) + ν CC_{R1} (10)
42	880	845	39.8	842 s	γ CH_{R1} (62)
43	943	906	7.3		γ $C_{16}H_{17}$ (59) + γ CH_{R2} (21)
44	968	930	0.2	923 w	γ CH_{R2} (84)
45	974	936	2.5		γ CH_{R2} (57) + γ $C_{16}H_{17}$ (23)
46	987	948	0.4	941 w	γ CH_{R1} (85)
47	996	957	0.8	961 w	γ CH_{R1} (87)
48	1019	979	5.6		ν C_{18}–C_{19} (15) + β CC_{R2} (13) + β CC_{R1} (13)
49	1025	985	0.3		β CCC_{R2} (43) + ν CC_{R2} (28)
50	1034	994	0.1		β CCC_{R1} (39) + ν CC_{R1} (35)
51	1068	1026	83.0	1032 s	ν O–CH_3 (76) + ν CC_{R2} (10)
52	1132	1087	109.9		ν CC_{R1} (30) + ν C_{28}-NO_2 (25) + β CH_{R1} (22)
53	1142	1097	6.2		β CH_{R1} (62) + ν CC_{R1} (24)
54	1152	1106	6.6	1112 m	β CH_{R2} (56) + ν CC_{R2} (20)
55	1176	1130	0.7		t CH_2 of CH_3 (99)
56	1209	1161	265.7		β CH_{R2} (60) + ν CC_{R2} (14)
57	1211	1164	16.4		r CH_3 (82)
58	1218	1170	23.0	1189 sh	β CH_{R1} (61) + ν CC_{R1} (24)
59	1242	1194	12.2	1196 w	β CH (24) + ν CC_{R2} (19) + ν CC (17)
60	1287	1237	1.5		ν C_{21}–C_{18} (39) + ν C_1–C_{16} (19)
61	1317	1265	444.8	1263 s	ν CO (47) + ν CC_{R2} (18) + β CH_{R2} (10)
62	1326	1274	1.6		β CH_{R1} (55) + ν CC_{R1} (22)
63	1349	1296	0.6		β CH_{R2} (44) + β CH_{R1} (20)
64	1354	1301	83.8		ν CC_{R2} (28) + β CH_{R2} (20)
65	1372	1318	168.8		ν CC_{R1} (40) + ν CC_{R2} (36)
66	1392	1337	705.2	1332 vw	ν_{sym} NO_2 (90)
67	1409	1354	43.4		β $C_{16}H_{17}$ (42) + ν C_{18}–C_{16} (15) + ν CC_{R1} (10)
68	1456	1399	6.9		ν CC_{R1} (32) + β CH_{R1} (29)
69	1473	1415	10.2		ν CC_{R2} (39) + β CH_{R2} (34)
70	1490	1431	16.1	1423 sh	ω CH_3 (85)
71	1506	1447	7.0		ρ CH_2 of CH_3 (75) + Γ COCH (20)
72	1516	1457	74.6		ρ CH_2 of CH_3 (83) + Γ COCH (12)
73	1534	1474	7.4		β CH_{R1} (59) + ν CC_{R1} (30)
74	1559	1498	142.7		β CH_{R2} (45) + ν CC_{R2} (22) + ν CO (10)
75	1604	1541	110.5		ν CC_{R2} (28) + ν C_{18}–C_{16} (17) + ν CC_{R1} (15) + ν_{asym} NO_2 (12)

Table 2 (*Continued*)

Mode no.	Unscaled Freq.	Scaled Freq.[a]	$I^{Infrared}$	FT-IR	TED[b] (≥10%)
76	1609	1546	73.5	1512 w	ν_{asym} NO_2 (32) + ν CC_{R1} (28) + ν CC_{R2} (22)
77	1626	1562	492.6		ν C_{18}–C_{16} (27) + ν CC_{R2} (16) + β $C_{16}H_{17}$ (11)
78	1655	1590	5.2	1580 s	ν CC_{R1} (54) + ν C_{18}–C_{16} (10)
79	1663	1598	149.4		ν_{asym} NO_2 (40) + ν CC_{R1} (26)
80	1670	1605	120.6		ν CC_{R2} (50) + ν C_{18}–C_{16} (11)
81	2324	2233	33.0	2213 m	ν C≡N (100)
82	3028	2909	69.4	2842 m	ν_{sym} CH_2 of CH_3 (100)
83	3095	2974	32.5	2941 m	ν_{asym} CH_2 of CH_3 (100)
84	3161	3037	23.8		ν_{asym} CH_3 (100)
85	3174	3050	5.8		ν C_{16}–H_{17} (98)
86	3184	3059	11.4		ν CH_{R2} (99)
87	3210	3084	3.7		ν CH_{R1} (98)
88	3212	3086	1.0	3086 m	ν CH_{R1} (96)
89	3219	3093	7.5		ν CH_{R2} (99)
90	3224	3098	8.8		ν CH_{R2} (99)
91	3246	3119	1.0		ν CH_{R1} (98)
92	3247	3120	1.2		ν CH_{R1} (95)
93	3248	3120	3.9		ν CH_{R2} (100)

R1 and R2; first and second ring, ν; stretching, β; in plane bending, γ; out of plane bending, ρ; scissoring, Γ; torsion, ω; wagging, r; rocking, t; twisting. [Frequency (cm^{-1}), IR intensities; I_{IR} ($K\,mmol^{-1}$)].

[a] Scale factor of 0.9608 was used for B3LYP/6-31G(d,p) basis set [17].

[b] Total energy distribution.

The sharp band in the region of 2210–2270 cm^{-1} is easily assigned to the characteristic C≡N stretching mode [29]. For 3-(4MP)-2-(4-NP)-AN, the strong FT-IR band at 2213 cm^{-1} was assigned to C≡N stretching vibration which has a good correlation with literature [29–31]. This mode (mode 81) appears in our calculation at 2233 cm^{-1}. The TED of this vibration is 100%. Because of the wide spectral range and poor IR intensity C–C–C≡N bending does not offer practical application as a characteristic frequency [29].

Empirical assignments of vibrational modes for peaks in the fingerprint region are difficult. In the wavenumber region of 600–1660 cm^{-1}, the spectrum observed in the experiments closely resembles the calculated spectrum, except for differences in details.

NO_2 asymmetric and symmetric stretching vibrations generally give rise to bands in the regions 1500–1570 cm^{-1} and 1300–1370 cm^{-1} in nitrobenzene and substituted nitrobenzenes, respectively [26,29]. We assigned the frequencies at 1512 and 1332 cm^{-1} to NO_2 asymmetric and NO_2 symmetric stretching vibrations, respectively. The theoretically scaled values at 1546 and 1337 cm^{-1} exactly correlate with experimental observations. The TED of this mode is contributing 32% for NO_2 asymmetric stretching and 90% for NO_2 symmetric stretching.

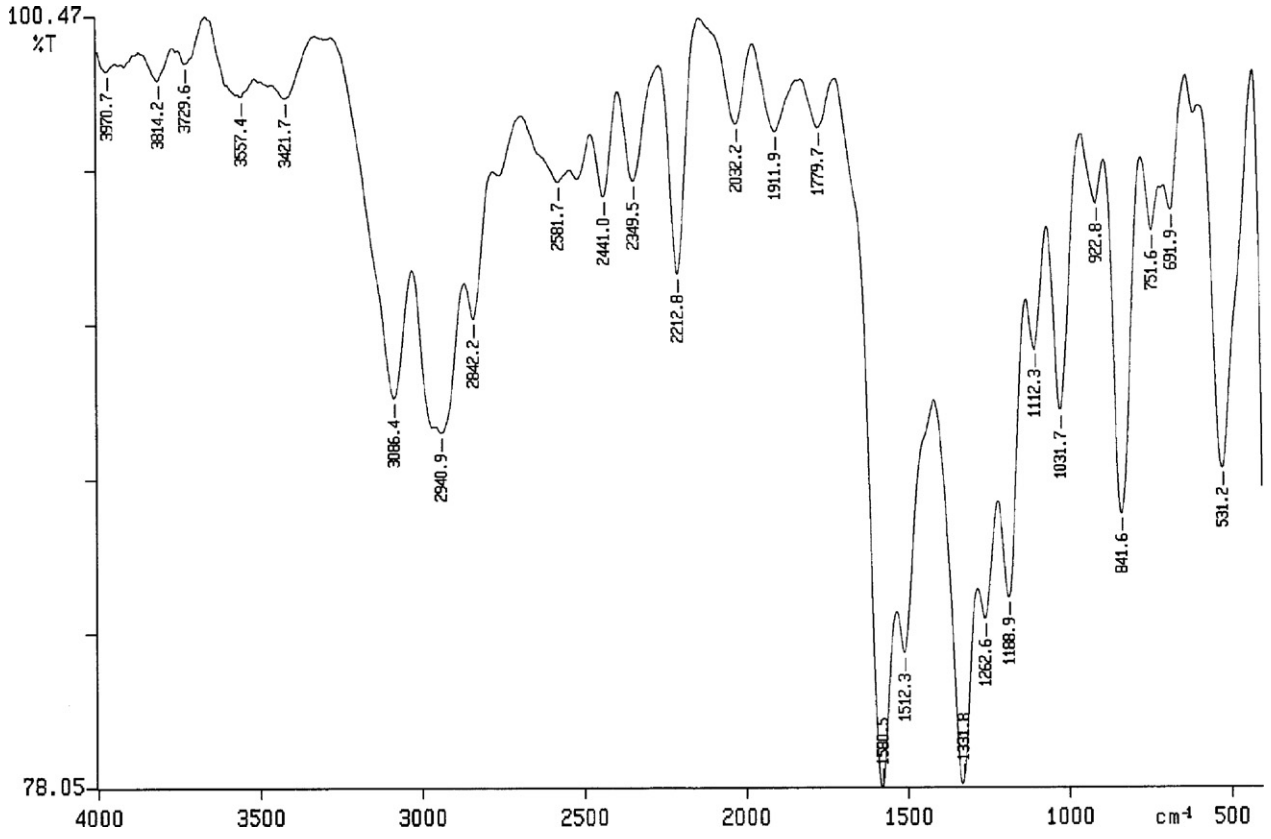

Fig. 3. The experimental Infrared spectrum of title molecule.

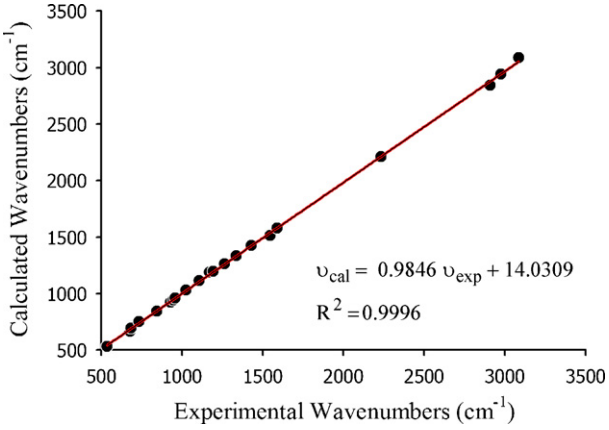

Fig. 4. Correlation graphic of calculated and experimental frequencies of title molecule.

The ring stretching vibrations which are highly characteristic of the aromatic ring itself, are very much important in the spectrum of benzene and its derivatives. The ring carbon–carbon stretching vibrations occur in the region 1450–1650 cm^{-1} [26,29] In the present work, the CC stretching modes are observed at 1580 and 1512 cm^{-1} in the FT-IR spectrum for R1 and R2 rings, respectively. The CC stretching vibrations calculated at 1590 cm^{-1} is in excellent agreement with experimental observations of 1580 cm^{-1}. The theoretically calculated CCC in-plane and out-of-plane bending modes have been obtained to be consistent with the recorded spectral values. The remaining modes are gathered in Table 2.

We drawn correlation graphics between the experimental and calculated wavenumbers obtained by DFT/B3LYP/6-31G(d,p) method. The correlation graphic describes the harmony between the calculated and experimental wavenumbers (Fig. 4). As can be seen from Fig. 4, experimental fundamentals have a good correlation with B3LYP. The relations between the calculated and experimental wavenumbers are linear and described by the following equation:

$$\upsilon_{cal} = 0.9846\upsilon_{exp} + 14.0309$$

We calculated RMS value ($R^2 = 0.9996$) between the calculated and experimental wavenumbers. As a result, the performances of the B3LYP method with respect to the prediction of the wavenumbers within the molecule were quite close.

3.3. Electronic absorption spectra and frontier molecular orbitals (FMOs)

In order to understand electronic transitions of compound, TD-DFT calculations on electronic absorption spectrum in chloroform were performed. The experimental and theoretical (where the wave length is plotted against the molar absorptivity of solution) UV–vis spectrum of 3-(4MP)-2-(4-NP)-AN is shown in Fig. 5 and Fig. S2 (Supplementary Information), was measured and calculated in chloroform solution. It is observed that the absorption band

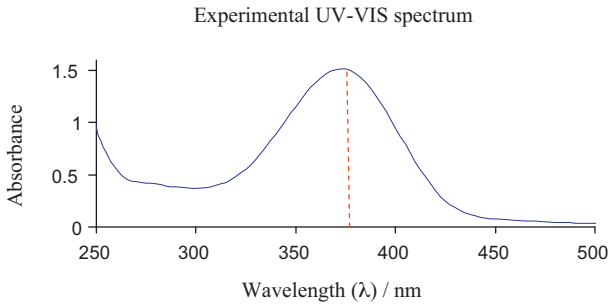

Fig. 5. The UV–vis spectrum of title molecule (in chloroform).

Table 4
Calculated energies values of 3-(4MP)-2-(4-NP)-AN in gas phase and chloroform.

TD-DFT/B3LYP/6-31G(d,p)	Chloroform	Gas
E_{total} (Hartree)	−951.9944313	−951.87767942
E_{HOMO} (eV)	−5.9898	−6.1234
E_{LUMO} (eV)	−2.7495	−2.7285
$\Delta E_{HOMO-LUMO\ gap}$ (eV)	3.2404	3.3949
E_{HOMO-1} (eV)	−7.2761	−7.4601
E_{LUMO+1} (eV)	−1.8977	−1.8879
$\Delta E_{HOMO-1-LUMO+1\ gap}$ (eV)	5.3784	5.5721
Dipole moment μ (Debye)	9.4019	7.9294

centered at 378 nm (calculated at 424.08 and 329.12 nm in chloroform and at 390.73 and 334.55 nm in gas phase). The experimental and computed electronic values, such as absorption wavelength (λ), excitation energies (*E*), and oscillator strengths (*f*) are tabulated in Table 3. The major contributions of the transitions were designated with the aid of SWizard program [32]. The experimental band at 378 nm is attributed mainly to a HOMO → LUMO transition is predicted as $\pi \rightarrow \pi^*$ transition. In view of calculated absorption spectrum, the maximum absorption wavelength corresponds to the electronic transition from the HOMO to LUMO with 89% contribution. The other wavelength, excitation energies, oscillator strength and calculated counterparts with major contributions can be seen in Table 3.

The total energy, energy gap and dipole moment have influence on the stability of a molecule. We have performed optimization in order to investigate the energetic behavior and dipole moment of title compound in solvent and gas phase. The total energy, dipole moment and frontier molecular orbital energies have been calculated. Results obtained in solvent and gas phase are listed in Table 4.

Both HOMO and LUMO are the main orbital taking part in chemical reaction. The HOMO energy characterizes the ability of electron giving, LUMO characterizes the ability of electron accepting, and the gap between HOMO and LUMO characterizes the molecular chemical stability [33]. Surfaces for the frontier orbitals were drawn to understand the bonding scheme of present compound. Here, four important molecular orbitals (MOs) were examined for 3-(4MP)-2-(4-NP)-AN: the second highest and highest occupied MOs and the lowest and the second lowest unoccupied MOs which are denoted as HOMO − 1, HOMO, LUMO and LUMO + 1, respectively. The features of these MOs can be seen in Fig. 6. The positive phase is red

Table 3
Experimental and calculated absorption wavelength λ (nm), excitation energies E (eV) and oscillator strengths (*f*) of 3-(4MP)-2-(4-NP)-AN in gas phase and chloroform.

Experimental	TD-DFT/B3LYP/6-31G(d,p)						
Chloroform	Gas			Chloroform			Major contribution[a]
λ (nm)	λ (nm)	*E* (eV)	(*f*)	λ (nm)	*E* (eV)	(*f*)	
378 (3.2800 eV)	390.73	3.1731	0.7779	424.08	2.9236	0.8404	H → L (89%)
	334.55	3.7060	0.0020	329.12	3.7671	0.3412	H → L + 1(85%)

[a] H: HOMO, L: LUMO.

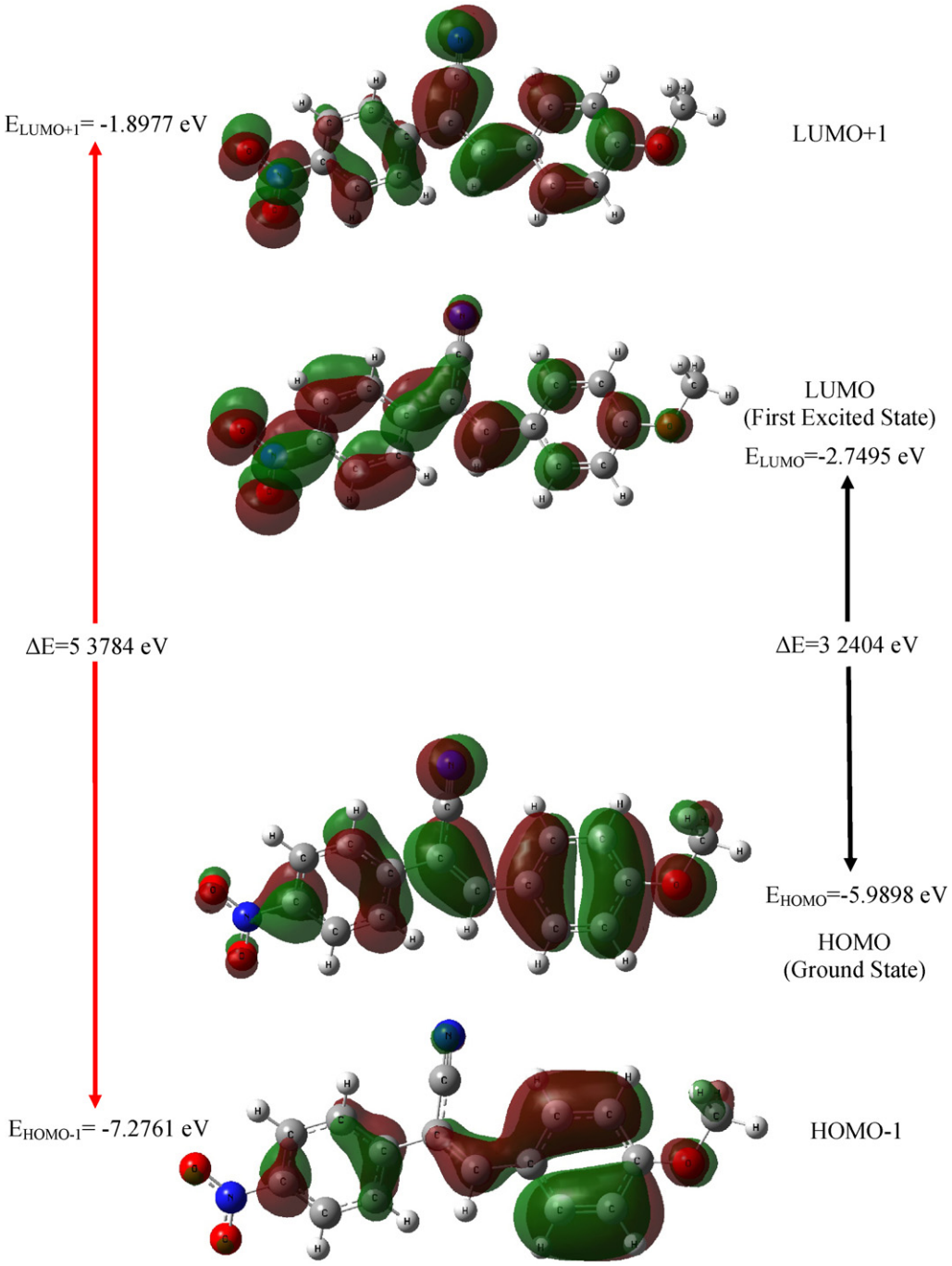

Fig. 6. The HOMO and LUMO distribution of title molecule by using B3LYP.

and the negative one is green. According to Fig. 6, the HOMO of 3-(4MP)-2-(4-NP)-AN presents a charge density localized on some carbon atoms of ring1 and all carbon atoms of the ring2, C═C bond, ≡N and O atoms, H atoms of CH_3, but LUMO is characterized by a charge distribution on some carbon atoms of the ring2, all carbon atoms of the ring1 and NO_2 group. The energy gap between HOMO and LUMO, is a critical parameter in determining molecular electrical transport properties because it is a measure of electron conductivity. The energy gap between HOMO and LUMO describes the chemical reactivity, optical polarizability, kinetic stability, and chemical softness–hardness of a molecule. The chemical hardness is a good indicator of the chemical stability. The molecules having a small energy gap are known as soft and having a large energy gap are known as hard molecules. The hard molecules are not more polarizable than the soft ones because they need big energy to excitation [34]. The hardness (η) value of a molecule is formulated by the following equation [35].

$$\eta = \frac{-\varepsilon_{HOMO} + \varepsilon_{LUMO}}{2}$$

where ε_{HOMO} and ε_{LUMO} are the energies of the HOMO and LUMO orbitals. The value of energy gap between the HOMO and LUMO is 3.3949 eV and the value of hardness is 1.6974 eV for the title molecule (Table 4). The chemical hardness value is a little bit smaller than that of (E)-4-methoxy-2-[(p-tolylimino)methyl]phenol molecule [34], which is a Schiff based compound (1.842 eV), that is a hardness molecule. Furthermore, in going from the gas phase to the solvent phase, the chemical hard-

Table 5
Experimental and theoretical, ^{1}H and ^{13}C isotropic chemical shifts (with respect to TMS, all values in ppm) of 3-(4MP)-2-(4-NP)-AN, in gas phase and chloroform.

Atom	Exp.	B3LYP		Atom	Exp.	B3LYP	
	$CDCl_3$	$CDCl_3$	Gas		$CDCl_3$	$CDCl_3$	Gas
H(7)	7.85	7.57	7.28	C(1)	125.65	122.27	122.50
H(8)	7.04	7.21	7.04	C(2)	131.96	134.15	132.99
H(9)	7.04	7.11	6.92	C(3)	114.64	113.78	113.50
H(10)	7.98	9.23	9.36	C(4)	162.37	158.12	157.30
H(13)	3.92	4.13	4.11	C(5)	114.64	107.16	106.66
H(14)	3.92	3.84	3.77	C(6)	131.96	126.18	126.30
H(15)	3.92	3.83	3.77	C(12)	55.56	53.44	53.45
H(17)	7.63	7.56	7.21	C(16)	141.08	145.07	141.99
H(25)	7.85	7.83	7.56	C(18)	106.10	101.24	103.49
H(27)	7.98	8.03	7.99	C(19)	117.77	112.52	110.55
H(29)	8.33	8.55	8.43	C(21)	145.06	141.15	140.04
H(30)	8.33	8.59	8.51	C(22)	126.33	120.17	119.21
				C(23)	126.33	123.35	123.55
				C(24)	124.34	121.04	120.57
				C(26)	124.34	121.18	121.07
				C(28)	147.45	143.61	143.15

ness increases in parallel with the increasing value of the energy gap and molecule becomes more stable [34]. This result shows good agreement with literature data [34,36].

The dipole moment in a molecule is another important electronic property which results from non-uniform distribution of charges on the various atoms in a molecule. It is mainly used to study the intermolecular interactions involving the van der Waals type dipole–dipole forces, etc., because bigger the dipole moment, stronger will be the intermolecular interactions [37]. Furthermore, we can say that in going from the gas phase to the solvent phase, the dipole moment value increases (Table 4).

3.4. NMR spectra

The isotropic chemical shifts are frequently used as an aid in identification of reactive ionic species. It is recognized that accurate predictions of molecular geometries are essential for reliable calculations of magnetic properties. Therefore, molecular structure of the mentioned compound was optimized by using B3LYP method in conjunction with 6-31G(d,p). Then, gauge-including atomic orbital (GIAO) ^{13}C and ^{1}H chemical shift calculations of the compound were made. The GIAO [20,38] method is one of the most common approaches for calculating nuclear magnetic shielding tensors. For the same basis set size GIAO method is often more accurate than those calculated with other approaches [21].

The experimental (in chloroform) and calculated (in chloroform and gas phase) values for ^{1}H and ^{13}C NMR are shown in Table 5. Relative chemical shifts were estimated by using the corresponding TMS shielding calculated in advance at the same theoretical level as the reference. ^{1}H and ^{13}C chemical shift values (with respect to TMS) have been calculated for the optimized structure of the title compound and compared to the experimental chemical shift values. Taking into account that the range of ^{13}C NMR chemical shifts for a typical organic molecule usually is >100 ppm [39,40], the accuracy ensures reliable interpretation of spectroscopic parameters. In the present paper, ^{13}C NMR chemical shifts in the ring for the title compound are >100 ppm, as they would be expected (Table 5). Oxygen and nitrogen atoms show electronegative property and oxygen atom has also more electronegative property than nitrogen atom. The oxygen and nitrogen atoms polarize the electron distribution in its bond to carbon and decrease the electron density at the ring carbon. Therefore, the chemical shifts values of C(4) and C(28) bonded to the oxygen and nitrogen atoms show calculated ^{13}C chemical shifts that are too high in the rings. The chemical shift values of C4 and C28 which are in the ring has been observed at 162.37 and 147.45 ppm (C–O and C–N) and calculated 158.12 and 143.61 ppm in chloroform (157.30 and 143.15 ppm in gas phase), respectively. Similarly, other five carbons' peaks in the rings are observed from 114.64 to 145.06 ppm and are calculated from 107.16 to 141.15 ppm in chloroform (from 106.66 to 140.04 ppm in gas phase).

In the ^{1}H NMR spectrum just one type of protons appears at 3.92 ppm as a singlet (O–CH_3), where as the chemical shift value of 3.83, 3.84 and 4.13 ppm in chloroform have been determined, the values are listed in Table 5. Signals for protons in the rings were observed at 7.04–8.33 ppm. The signal at 7.63 ppm (calculated at 7.56 and 7.21 ppm in chloroform and gas phase, respectively) is due to olefinic H (H_{17}). The H atom is the smallest of all atoms and mostly localized on the periphery of molecules; therefore their chemical shifts would be more susceptible to intermolecular interactions in the aqueous solutions as compared to that for other heavier atoms.

The relations between the calculated and experimental wavenumbers chemical shifts (δ_{exp}) and magnetic isotropic shielding tensors (σ) are usually linear and described by the following equation:

$$\delta_{cal}(ppm) = 0.9745\delta_{exp} + 0.1278 (R^2 = 0.9986)$$

In present study, the following linear relationships were obtained for ^{1}H and ^{13}C chemical shifts.

$$^1H: \delta_{cal}(ppm) = 1.0512\delta_{exp} - 0.2083$$

$$^{13}C: \delta_{cal}(ppm) = 1.0068\delta_{exp} - 4.0416$$

The performance of the B3LYP method with respect to the prediction of the relative isotropic chemical shifts within the molecule was quite close. However, ^{13}C calculations gave a slightly better coefficient and lower standard error (R^2 = 0.9844) than for ^{1}H (R^2 = 0.9624) chemical shifts. The correlations between the experimental and calculated chemical shifts obtained by DFT/B3LYP method are shown in Fig. 7. As can be seen from Table 5 and Fig. 7, there is a good agreement between experimental and theoretical chemical shift results for the title compound.

3.5. Thermodynamic properties

The values of some thermodynamic parameters (such as zero-point vibrational energy, thermal energy, specific heat capacity, rotational constants, and entropy) of title molecule by DFT/B3LYP/6-31G(d,p) method are listed in the Table 6. The variation in Zero-Point Vibrational Energies (ZPVEs) seems to be

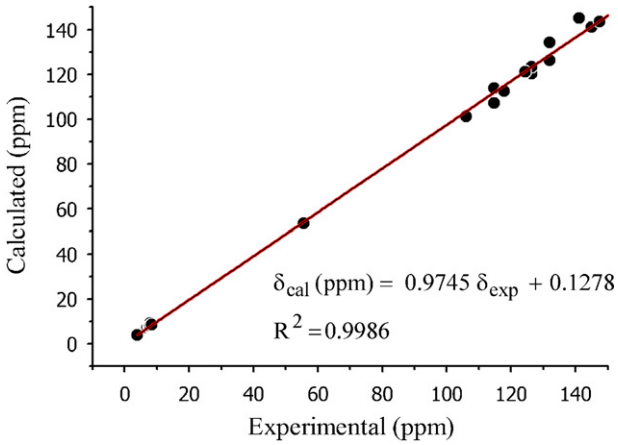

Fig. 7. Correlation graphic of calculated and experimental chemical shifts of title molecule.

Table 6
The calculated thermo dynamical parameters of in gas at 298.15 K.

Basic set	B3LYP/6-31G(d,p)
SCF energy (a.u.)	−951.87767942
Zero point vib. energy (kcal mol^{-1})	156.43152
Rotational constants (GHz)	1.11498
	0.09897
	0.09161
Specific heat (C_v) (cal mol^{-1} K^{-1})	67.882
Entropy (S) (cal mol^{-1} K^{-1})	142.354

Table 7
Thermodynamic properties at different temperatures at the B3LYP/6-31G(d,p) level for 3-(4MP)-2-(4-NP)-AN.

T (K)	$C_{p,m}^\circ$ (cal mol^{-1} K^{-1})	S_m° (cal mol^{-1} K^{-1})	ΔH_m° (kcal mol^{-1})
100	28.581	91.607	2.003
150	38.140	105.802	3.770
200	48.002	118.689	6.021
250	58.133	130.929	8.774
298.15	67.882	142.354	11.904
300	68.252	142.787	12.034
350	78.022	154.355	15.792
400	87.182	165.644	20.024
450	95.587	176.640	24.696
500	103.197	187.321	29.768
550	110.039	197.673	35.202
600	116.178	207.689	40.959

significant. On the basis of vibrational analysis, the standard statistical thermodynamic functions: standard heat capacity ($C_{p,m}^\circ$) standard entropy (S_m°) and standard enthalpy changes (ΔH_m°) for the title compound were obtained from the theoretical harmonic frequencies and listed in Table 7.

From Table 7, it can be seen that these thermodynamic functions are increasing with temperature ranging from 100 to 600 K due to the fact that the molecular vibrational intensities increase with temperature [41]. The correlation equations between heat capacities, entropies, enthalpy changes and temperatures were fitted by quadratic formulas and the corresponding fitting factors (R^2) for these thermodynamic properties are 0.9994, 0.9999 and 0.9999, respectively. The corresponding fitting equations are as follows and the correlation graphics of those are shown in Figs. 8–10.

$$C_{p,m}^\circ = 4.2405 + 0.2409T - 8.8185 \times 10^{-5}T^2 \quad (R^2 = 0.9994)$$

$$S_m^\circ = 64.6573 + 0.2829T - 7.4818 \times 10^{-5}T^2 \quad (R^2 = 0.9999)$$

$$\Delta H_m^\circ = -0.4765 + 0.0146T + 9.1334 \times 10^{-5}T^2 \quad (R^2 = 0.9999)$$

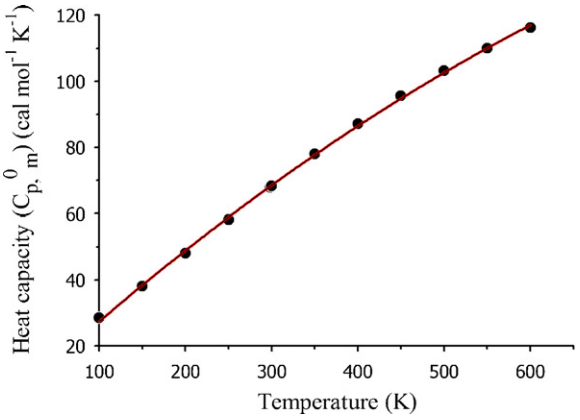

Fig. 8. Correlation graphic of heat capacity and temperature for the title molecule.

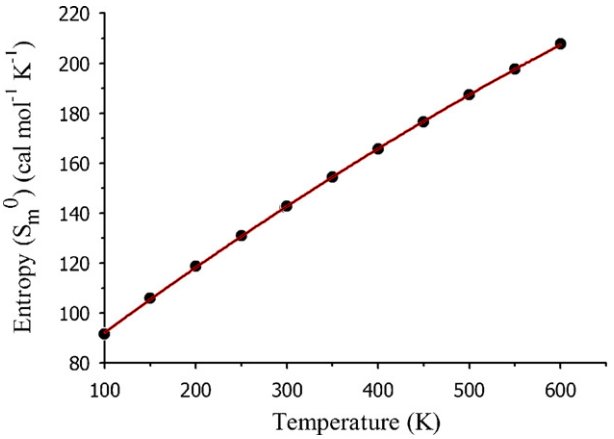

Fig. 9. Correlation graphic of entropy and temperature for the title molecule.

All the thermodynamic data supply helpful information for the further study on the 3-(4MP)-2-(4-NP)-AN. They can be used to compute the other thermodynamic energies according to relationships of thermodynamic functions and estimate directions of chemical reactions according to the second law of thermodynamics in Thermochemical field [41].

Notice: all thermodynamic calculations were done in gas phase and they could not be used in solution.

3.6. Nonlinear optical (NLO) effects

In the recent years, because of potential applications in modern communication technology, data storage, telecommunication, and optical signal processing, a large number research of new materials exhibiting efficient nonlinear optical (NLO) properties has been of great interest [42–46]. It is known that the significance of the polarizability and the first hyperpolarizability of molecular systems is dependent on the efficiency of electronic communication between acceptor and the donor groups as that will be the key to intra molecular charge transfer [34,47]. The acceptor and donor groups have an important role in the polarizability and first hyperpolarizability. The large value of first hyperpolarizability, which is the measure of the NLO activity of the molecular system, is associated with the resulting from the electron cloud movement through π conjugated frame work from electron donor to electron acceptor groups [48]. The polar properties of the title molecule were calculated at the DFT/B3LYP/6-31G(d,p) level. The components of the dipole moments μ (Debye), static polarizability components

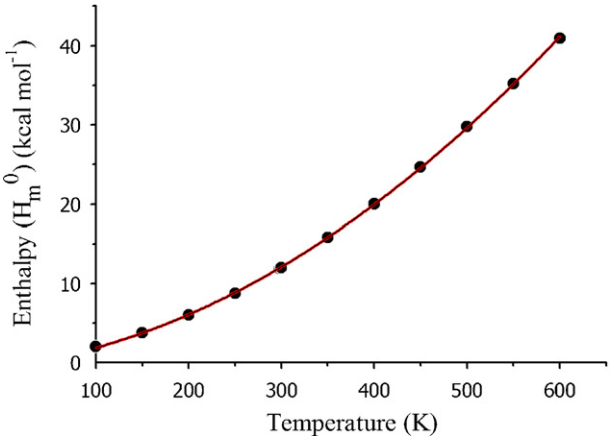

Fig. 10. Correlation graphic of enthalpy and temperature for the title molecule.

Table 8
The dipole moments components μ (D), static polarizability components α (a.u.), the average polarizability α_0 (Å), the anisotropy of the polarizability $\Delta\alpha$ (Å), and the first hyperpolarizability components β (a.u.), the first hyperpolarizability β_0 ($\times 10^{-29}$ cm^5 esu^{-1}) of 3-(4MP)-2-(4-NP)-AN.

μ_x	2.351087	β_{xxx}	−7454.627626
μ_y	−0.149940	β_{xxy}	−33.593974
μ_z	2.045083	β_{xyy}	49.688041
μ_0	3.119688	β_{yyy}	−5.113166
α_{xx}	375.162848	β_{xxz}	−3836.841045
α_{xy}	8.091439	β_{xyz}	−33.318967
α_{yy}	84.134560	β_{yyz}	0.109298
α_{xz}	109.679948	β_{xzz}	−1837.480426
α_{yz}	−25.908897	β_{yzz}	−10.074198
α_{zz}	250.623800	β_{zzz}	−784.475027
α_0	35.070108	β_x	−9242.420010
$\Delta\alpha$	103.337442	β_y	−48.781337
		β_z	−4621.206774
		β_0	8.927380

α (a.u.), the average polarizability (or linear polarizability) α_0 (Å), the anisotropy of the polarizability $\Delta\alpha$ (Å), and the first hyperpolarizability components β (a.u.), the first hyperpolarizability β_0 ($\times 10^{-29}$ cm^5 esu^{-1}) of 3-(4MP)-2-(4-NP)-AN can be seen in Table 8. The $\mu_0, \alpha_0, \Delta\alpha, \beta$, and β_0 of title molecule can be calculated by using the following equations, respectively [34,49,50].

$$\mu_0 = (\mu_x^2 + \mu_y^2 + \mu_z^2)^{1/2}$$

$$\alpha_0 = \frac{(\alpha_{xx} + \alpha_{yy} + \alpha_{zz})}{3}$$

$$\Delta\alpha = \frac{1}{\sqrt{2}}[(\alpha_{xx} - \alpha_{yy})^2 + (\alpha_{yy} - \alpha_{zz})^2 + (\alpha_{zz} - \alpha_{yy})^2 + 6\alpha_{xx}^2]^{1/2}$$

$$\beta_x = \beta_{xxx} + \beta_{xyy} + \beta_{xzz}$$

$$\beta_y = \beta_{yyy} + \beta_{xxy} + \beta_{yzz}$$

$$\beta_z = \beta_{zzz} + \beta_{xxz} + \beta_{yyz}$$

$$\beta_0 = (\beta_x^2 + \beta_y^2 + \beta_z^2)^{1/2}$$

The calculated values of the μ, α_0, $\Delta\alpha$ and β_0 of 3-(4MP)-2-(4-NP)-AN are 3.119688 Debye, 35.070108 Å^3, 103.337442 Å^3 and 8.927380×10^{-29} cm^5 esu^{-1}, respectively. It is well known that the substituent influence the polarity of the molecules. The μ, α_0 and β_0 value of the investigated compound are all bigger than those of urea (μ, α_0, and β_0 of urea are 1.392196 Debye, 3.873427 Å^3 and $3.850676203 \times 10^{-31}$ cm^5 esu^{-1} obtained with the same method). The total dipole moment of title compound is ca. 2 times greater than those of urea, and the average polarizability of title compound is ca. 9 times greater than those of urea. Theoretically, the first-order hyperpolarizability of the investigated compound is ca. 231 times magnitude of urea, which is also larger than the values reported previously [34,43,48–53]. That is to say, the title compound can be used as a good candidate of NLO materials.

4. Conclusion

The 3-(4-Methoxy-phenyl)-2-(4-nitro-phenyl)-acrylonitrile was synthesized and several properties were studied using experimental techniques and tools derived from the density functional theory. The vibrational FT-IR spectrum of molecule was recorded and assigned with the aid of the experimental and computed vibrational wavenumbers and their TED. The magnetic properties of the title compound were observed and calculated. The chemical shifts were compared with experimental data, showing a very good agreement both for ^{13}C and ^{1}H. The electronic properties were also calculated and experimental electronic spectrum was recorded with help of UV–vis spectrometer. The experimental band at 378 nm is attributed mainly to a HOMO → LUMO transition is predicted as $\pi \rightarrow \pi^*$ transition. The comparison of the predicted bands with the experimental bands was done and shows an acceptable general agreement. The correlations between the statistical thermodynamics and temperature are also obtained. It is seen that the heat capacities, entropies and enthalpies increase with the increasing temperature owing to the intensities of the molecular vibrations increase with increasing temperature. Furthermore, the polarizability, the first hyperpolarizability and total dipole moment properties of title molecule have been calculated and the results are discussed. The total linear polarizability and first-order hyperpolarizabilities calculated respectively present 35.070108 Å^3 and 8.927380×10^{-29} cm^5 esu^{-1} which imply that the title compound can be used as a good nonlinear optical material. The present quantum chemical study may further play an important role in understanding of dynamics of this molecule.

In summary, a very complete characterization of studied novel compound was given in the present paper. It has been shown; moreover, hybrid density functional calculations are able to supply a variety of very reliable molecular properties. We hope the results of this study will be of assistance to researchers to design and synthesis new materials.

Appendix A. Supplementary data

Supplementary data associated with this article can be found, in the online version, at doi:10.1016/j.saa.2011.07.076.

References

[1] J. Fabian, H. Hartmann, Light Absorption of Organic Colorants, Springer Verlag, Berlin, 1980.
[2] A.M. Asiri, Dyes Pigments 42 (1999) 209–213.
[3] A. Attia, M. Michael, Pharmazie 37 (1982) 551–553.
[4] M. Karabacak, M. Kurt, M. Cinar, A. Coruh, Mol. Phys. 107 (3) (2009) 253–264.
[5] J. Swaminathan, M. Ramalingam, H. Saleem, V. Sethuraman, M.T.N. Ameen, Spectrochim. Acta A 74 (2009) 1247–1253.
[6] P.B. Nagabalasubramanian, S. Periandy, S. Mohan, M. Govindarajan, Spectrochim. Acta A 73 (2009) 277–280.
[7] M. Karabacak, M. Cinar, S. Ermec, M. Kurt, J. Raman Spectrosc. 41 (2010) 98–105.
[8] M. Arivazhagan, V. Krishnakumar, R.J. Xavier, G. Ilango, V. Balachandran, Spectrochim. Acta A 72 (2009) 941–946.
[9] M. Samsonowicz, T. Hrynaszkiewicz, R. Sïwisłocka, E. Regulska, W. Lewandowski, J. Mol. Struct. 744–747 (2005) 345–352.
[10] A.M. Asiri, Bull. Korean Chem. Soc. 24 (4) (2003) 426–430.
[11] M.J. Frisch, et al., Gaussian 03, Revision B. 4, Gaussian Inc., Pittsburgh, PA, 2003.
[12] C. Lee, W. Yang, R.G. Parr, Phys. Rev. B 37 (1988) 785–789.
[13] A.D. Becke, J. Chem. Phys. 98 (1993) 5648–5652.
[14] M. Karabacak, E. Şahin, M. Cinar, İ. Erol, M. Kurt, J. Mol. Struct. 886 (2008) 148–157.
[15] J.B. Foresman, E. Frisch, Exploring Chemistry with Electronic Structure Methods: A Guide to Using Gaussian, Gaussian, Pittsburgh, PA, 1993.
[16] A.P. Scott, L. Radom, J. Phys. Chem. 100 (1996) 16503–16513.
[17] NIST Chemistry Webbook, IR database, http://srdata.nist.gov/cccbdb.
[18] J. Baker, A.A. Jarzecki, P. Pulay, J. Phys. Chem. A 102 (1998) 1412–1424.
[19] SQM version 1.0, Scaled Quantum Mechanical Force Field, 2013 Green Acres Road, Fayetteville, Arkansas 72703.
[20] K. Wolinski, J.F. Hinton, P. Pulay, J. Am. Chem. Soc. 112 (1990) 8251–8260.
[21] J.R. Cheeseman, G.W. Trucks, T.A. Keith, M.J. Frisch, J. Chem. Phys. 104 (1996) 5497–5509.
[22] A.M. Asiri, S.A. Khan, K.W. Tan, S.W. Ng, Acta Crystallogr. E66 (2010) o1733.
[23] M.A. Palafox, J.L. Nunez, M. Gil, J. Mol. Struct. (Theochem.) 593 (2002) 101–131.
[24] A. Altun, K. Gölcük, M. Kumru, J. Mol. Struct. (Theochem.) 625 (2003) 17–24.
[25] W.B. Tzeng, K. Narayanan, J.L. Lin, C.C. Tung, Spectrochim. Acta 55A (1999) 153–156.
[26] M. Silverstein, G.C. Basseler, C. Morill, Spectrometric Identification of Organic Compounds, Wiley, New York, 1981.
[27] N. Sundaraganesan, S. Ilakiamani, B.D. Joshua, Spectrochim. Acta A 67 (2007) 287–297.
[28] R. Shanker, R.A. Yadav, I.S. Singh, O.N. Singh, Indian J. Pure Appl. Phys. 23 (1985) 339–343.

[29] D. Lin–Vien, N.B. Colthup, W.G. Fateley, J.G. Grasselli, The Handbook of Infrared and Raman Characteristic Frequencies of Organic Molecules, Academic Press, Boston, MA, 1991.
[30] V. Krishnakumar, S. Dheivamalar, Spectrochim. Acta 71A (2008) 465–470.
[31] S. Sudha, N. Sundaraganesan, M. Kurt, M. Cinar, M. Karabacak, J. Mol. Struct. 985 (2011) 148–156.
[32] S.I. Gorelsky, SWizard Program Revision 4.5, University of Ottawa, Ottawa, Canada, 2010, http://www.sg.chem.net/.
[33] K. Fukui, Science 218 (1982) 747–754.
[34] B. Kosar, C. Albayrak, Spectrochim. Acta A 78 (2011) 160–167.
[35] R.G. Pearson, Proc. Natl. Acad. Sci. U.S.A. 83 (1986) 8440–8841.
[36] C. Albayrak, B. Kosar, S. Demir, M. Odabasoglu, O. Büyükgüngör, J. Mol. Struct. 963 (2010) 211–218.
[37] O. Prasad, L. Sinha, N. Misra, V. Narayan, N. Kumar, J. Pathak, J. Mol. Struct. 940 (2010) 82–86.
[38] R. Ditchfield, J. Chem. Phys. 56 (1972) 5688.
[39] H.O. Kalinowski, S. Berger, S. Braun, Carbon-13 NMR Spectroscopy, John Wiley and Sons, Chichester, 1988.
[40] K. Pihlaja, E. Kleinpeter (Eds.), Carbon-13 Chemical Shifts in Structural and Stereochemical Analysis, VCH Publishers, Deerfield Beach, 1994.
[41] J. Bevan Ott, J. Boerio-Goates, Calculations from Statistical Thermodynamics, Academic Press, 2000.
[42] R. Zhang, B. Dub, G. Sun, Y. Sun, Spectrochim. Acta A 75 (2010) 1115–1124.
[43] S. Yazıcı, Ç. Albayrak, İ. Gümrükçüoğlu, I. Şenel, O. Büyükgüngör, J. Mol. Struct. 985 (2011) 292–298.
[44] D.S. Chemia, J. Zyss, Non Linear Optical Properties of Organic Molecules and Crystal, Academic Press, New York, 1987.
[45] J. Zyss, Molecular Non Linear Optics, Academic Press, Boston, 1994.
[46] A. Ben Ahmed, H. Feki, Y. Abid, C. Minnot, Spectrochim. Acta A 75 (2010) 1315–1320.
[47] K. Amila, K.M. Jeewandara, S. de Nalin, J. Mol. Struct. Theochem. 686 (2004) 131.
[48] N. Sundaraganesan, J. Karpagam, S. Sebastian, J.P. Cornard, Spectrochim. Acta A 73 (2009) 11–19.
[49] D. Sajan, J. Hubert, V.S. Jayakumar, J. Zaleski, J. Mol. Struct. 785 (2006) 43–53.
[50] R. Zhang, B. Du, G. Sun, Y. Sun, Spectrochim. Acta A 75 (2010) 1115–1124.
[51] C. Ravikumar, I.H. Joe, V.S. Jayakumar, Chem. Phys. Lett. 460 (2008) 552–558.
[52] F.F. Jian, P. Zhao, L. Zhang, J. Zheng, J Fluorine Chem. 127 (2006) 63–67.
[53] Y. Sun, Q. Hao, L. Lu, X. Wang, X. Yang, Spectrochim. Acta A 75 (2010) 203–211.